



OPEN Research on bending-slip rib spalling and rib stability of extra-thick hard coal wall

Bo Xue^{1,2✉}, Yan Shang^{1,2}, Chen Wang³, Feitian Zhang^{1,2} & Yunfei Liu¹

In response to the frequent occurrence of coal face spalling affecting the working face production during the mining of extra-thick hard coal seams, this study investigates the characteristics of typical hard coal face damage. Coal face spalling is categorized into three stages: dynamic load influence, crack propagation, and bending instability phase. Employing the Rayleigh-Ritz method and the principle of stationary potential energy in conjunction with beam plate strength theory and maximum tensile stress strength theory, a displacement formula for coal face spalling has been developed. The formula has been validated using numerical simulation software. Additionally, a three-dimensional similitude modeling experimental platform was utilized to explore the development and failure patterns of spalling. Experimental results confirm the consistency between the theoretical derivation and the observed trajectories and locations of coal face spalling movement. The findings provide a theoretical foundation and technical reference for the management and prevention of spalling in extra-thick hard coal seam faces.

Keywords Extra-thick hard coal, Coal wall rib spalling, Slabbed spalling failure, Spalling prevention and control

Following the upgrade of equipment and the innovation of mining technology, the focus of resource extraction has gradually shifted to thick and extra-thick coal seams^{1–4}. The increase of mining height and exposed space in extra-thick coal seam makes the problem of coal wall spalling become one of the main factors restricting the safe mining of thick coal seam^{5–9}. Severe coal wall spalling not only disrupts normal production operations at the working face but also poses a significant threat to worker safety. Consequently, rib failure in extra-thick coal seams has emerged as a critical issue affecting the smooth progression of mining activities in recent years^{10–13}.

Investigating the mechanism of coal wall rib failure and mitigating its effects have become paramount technical challenges for ensuring safe and efficient production in large mining height environment. Numerous studies have been undertaken in this field recently^{14–18}. The article^{19,20} establishes a “wedge-shaped” sliding body stability model for “three soft” large mining face; the article²¹ analyzes the characteristics of coal wall disturbance with high integrity by combining with the “compression bar” theory; the article²² analyzed the risk of coal wall sliding and analyzed the depth of sliding coal wall sliding by Bishop method; the article^{23,24} proposed the form of “pulling-sliding” type of sliding gang in large mining height work; the article^{25,26} studied the morphology and mechanism of coal wall spalling in thick coal seam, and proposed the flexible reinforcement technology.

The aforementioned research has provided a comprehensive analysis of the rib spalling mechanism and spalling type in large mining walls, offering both theoretical insights and practical guidance for preventing and controlling rib failures in these environments^{27–30}. However, rib spalling is a process of interaction between the mechanical strength of the material and the spatial environment in which it is located. The practice of extra-thick coal wall mining shows that rib spalling at the site is often manifested as “plate cracking” or “tetragonal” style, and the occurrence of central fracture is huge^{31–35}. In the context of shear failure within extremely thick hard coal seams, it is crucial to consider the bending motion and energy release associated with the flexural failure of “pseudo-platelike” structures. This study innovatively adopts a layered plate perspective to analyze shear failure along coal faces, employing the Rayleigh-Ritz method supported by numerical and physical modeling experiments. The aim is to identify the initial location and extent of maximum flexural failure within the coal face. By doing so, this research seeks to provide a theoretical foundation for addressing shear failure in large-scale mining of extremely thick hard coal seams. Additionally, it offers managerial insights and preventive measures

¹Department of Civil Engineering, Ordos Institute of Technology, Ordos 017000, Inner Mongolia, China. ²Erdos Mining Area Geohazard Prevention and Geoenvironmental Protection Engineering Research Center, Ordos Institute of Technology, Ordos 017000, Inner Mongolia, China. ³School of Mining, Guizhou University, Guiyang 550025, China. ✉email: bxueedu@163.com

as technical references for ensuring the safe management of coal face shear failure under similar geological conditions.

The failure characteristics of large mining height of coal wall

Caojiatan Coal mine, located in Yulin, Shaanxi Province, is a subsidiary of Shaanxi Coal Group. The main mine exploits the 2–2 coal seam, with a coal thickness ranging from 8.04 to 12.7 m, averaging 11.22 m, featuring a near-horizontal stratigraphic layout for mining. Currently, the 122,107 working face is being mined with a design extraction height of 6 m and a caving height of 5 m. The roof over the 2–2 coal seam consists of sandstone, exhibiting a compressive strength of approximately 31~39 MPa. The coal seam itself shows a compressive strength of about 17.9~30.8 MPa, indicating its high hardness and firmness. The lithologic characteristics of the 2–2 coal seam and its roof and floor are illustrated in Fig. 1.

During the phase of periodic weighting of the roof, phenomenon such as spalling and rib breakage occur along the local coal wall. The spalling condition of the coal wall within the working face can be described as follows: At sites where rib spalling has occurred, the coal wall fractures into plates with longitudinal sliding. When ribs fail, longitudinal and transverse cracks within the coal wall, and upon exceeding the ultimate strength, the central portion of the slab slides down along the shear plane due to tensile stress. The thickness of the sliding slab typically ranges between 50~700 mm. Slide backward multiple hit the bottom of the rupture of coal block, plate crack block and is apart from the bottom is more close to the integrity, as shown in Fig. 2.

Analysis of coal plate cracking
Development of coal wall rib spalling

Based on the temporal factor, the process of coal wall rib spalling can be segmented into three phases: dynamic load influence, crack propagation, and bending instability phase. The specific analysis is as follows^{36,37}.

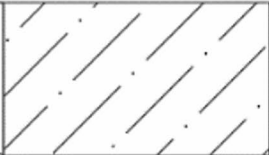

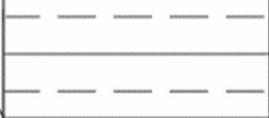


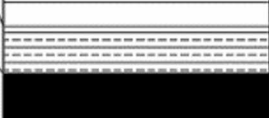

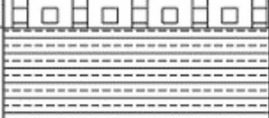
Number	Rock layer	Rockiness	Thickness/m
1		Medium sandstone	1 3
2		Fine Sandstone	1 7
3		Siltstone	1 2
4		Fine Sandstone	1 0
5		Siltstone	4
6		2-2 Coal	1 2
7		Sandy mudstone	4
8		Siltstone	8

Fig. 1. Coal rock mass histogram.

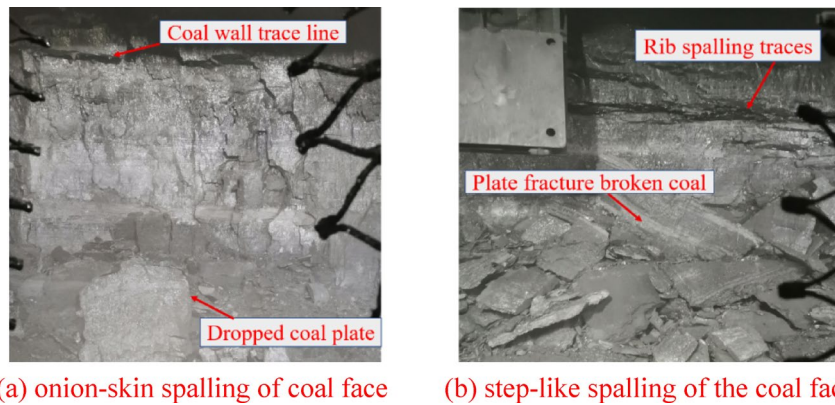
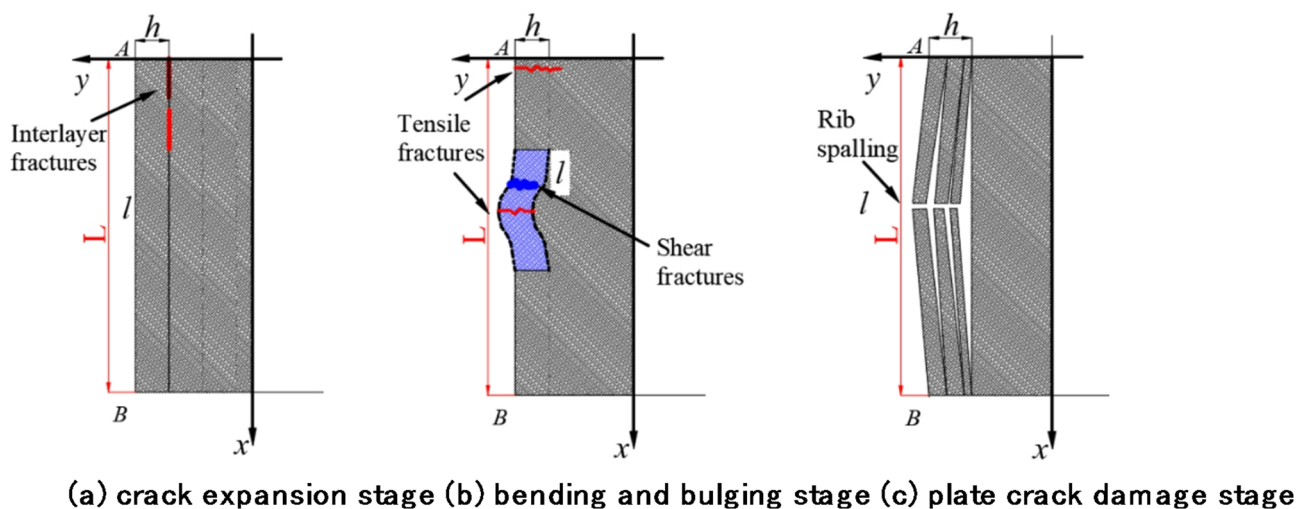


Fig. 2. Coal rock mass histogram.



(a) crack expansion stage (b) bending and bulging stage (c) plate crack damage stage

Fig. 3. Overall motion trend.

(1) dynamic load influence.

When the coal wall is not affected by mining, the strength of the interlayer structural plane is high, and the fracture penetration phenomenon does not occur only under the action of ground stress and overburden stress. After mining, the coal wall under the influence of mining produces cracks under the influence of triaxial stress.

(2) crack propagation.

This phase of coal wall cracks began, vertical cleat up under the maximum principal stress. Under the horizontal tensile stress caused by mining, the discontinuous longitudinal internal cutting groups in coal are extended and connected along the direction of maximum principal stress and parallel to the direction of excavation load surface to form a plate structure.

(3) bending instability phase.

In this stage, the plate-like structure progressively overcomes the friction resistance between its internal surfaces and adjacent structural planes, leading to a sliding motion. Due to the existence of stable coal body in the lower part, the coal plate reaches the bending equilibrium state. When the upper tension fissure is expanded through, the plate body breaks and becomes unstable, and the whole slide to the lower part, as shown in Fig. 3.

Analysis of plate bending section

Based on the aforementioned analysis regarding the evolution of coal wall movement along the seam, the deformation zone can be subdivided into two segments characterized by slip and bending. Consequently, three assumptions are proposed: ① The direction of cracking of the coal seam is vertical downward, due to the extra-thick hard coal body, bending stiffness is small, the stripping thickness is much smaller than the thickness of the coal body affected by mining; ② The coal seam contains obvious vertical cracks, the structure of the AC section

of the coal wall does not produce a tendency to bending, there is a tendency to downward movement as a whole, the middle of the point in the bending fracture, but the location is unknown; ③ In analyzing the motion of the monolithic body, factors such as frictional forces and energy dissipation are disregarded. The analysis focuses solely on the static equilibrium during the motion process, as illustrated in Fig. 4.

Assume that L is the overall length of the slab, l is the length of the bending section, x is the parallel level coordinate axis, y is the perpendicular level coordinate axis, and γ is the overall weight of the rock formation. The overall mechanical model diagram is shown in Fig. 4(a), and any micro-element body within the slip section AC is taken for force analysis, as shown in Fig. 4(b), which can be obtained from the geometric relationship:

$$\begin{cases} P_x = G \sin \theta \\ P_y = G \cos \theta = \sigma_N \end{cases} \quad (1)$$

$$\tau = \sigma_N \tan \varphi_s + c_s. \quad (2)$$

Where: σ_N is the positive stress at the level; τ is the shear strength of the coal wall along the layer; G is the self-weight of the coal block; c_s is the cohesive force; φ_s is the friction angle of the structural surface. The axial force at a point location P_{rx} on the surface is:

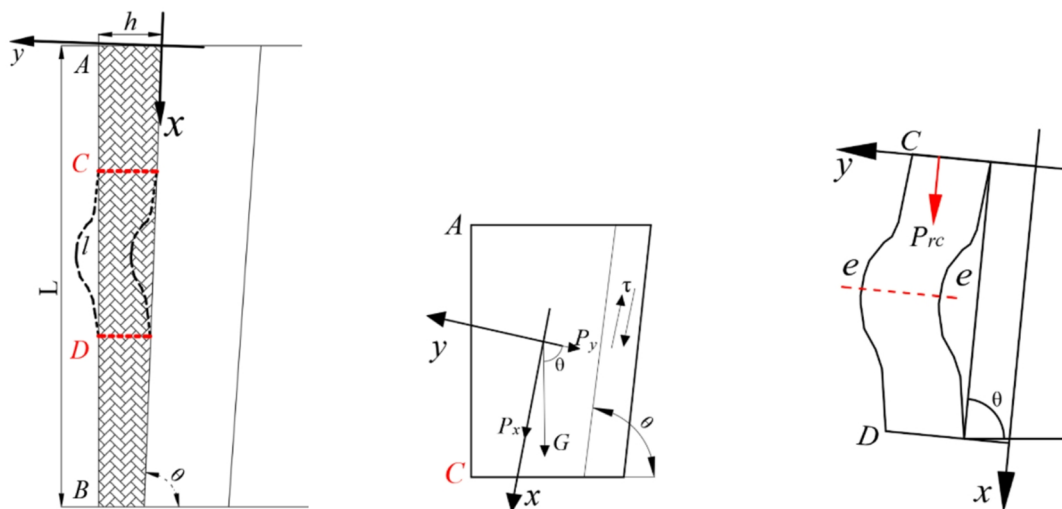
$$P_{rx} = \int_0^x (G \sin \theta - \tau) dx = \int_0^x (G \sin \theta - \sigma_N \tan \varphi_s - c_s) dx = (\gamma h \sin \theta - \gamma h \cos \theta \tan \varphi_s - c_s)x. \quad (3)$$

Analysing Eq. (3), if the uniaxial compressive strength of the coal body is less than the axial force, i.e., when $R_c < P_{rx}$, the rib spalling is in the form of pressure-shear damage in the AC section; if the compressive strength is much greater than the axial force; when $R_c \gg P_{rx}$, the AC section does not produce damage. Considering its limit state can be deduced from Eq. (3) the critical length of AC section, the critical length l_{rx} is:

$$l_{rx} = \frac{R_c}{(\gamma h \sin \theta - \gamma h \cos \theta \tan \varphi_s - c_s)}. \quad (4)$$

The coal wall will be damaged by pulling from the middle CD section of the coal wall if the coal wall is not damaged in the AC section. According to the physical constraint conditions of the plate body, the C end is regarded as a rigid slider, the D end is regarded as a fixed constraint, and the slider is limited to move freely only in the slip surface, and due to the constraint effect of the upper and lower coal bodies and the internal stress, the bending and bulging occurs along the normal outward direction of the unbroken plate body. Rayleigh-Ritz is used to establish the trial function, and the bending deformation shape function is constructed under satisfying the boundary conditions (Eq. (5)), where a is the displacement point of the shape function, and the equations are as follows:

$$\left. \begin{aligned} x = 0, y = 0, y' = 0 \\ x = l, y = 0, y' = 0 \end{aligned} \right\} \quad (5)$$



(a) holistic model (b) Mechanical Modelling of Slip Surfaces (c) Bending Mechanics Model

Fig. 4. Integral Mechanical Model and Slip Surface Model.

$$y = \frac{a}{2} \left(1 - \cos \frac{2\pi x}{l} \right). \quad (6)$$

Calculate the analytical formula of the total potential energy function of the bending model, the formula establishment process ignores the shear strain energy and the energy consumed by the slip of the coal plate along the main cleavage line, and the formula includes two parts: the deformation energy U and the work of the external force W , and the functional expression is as follows:

$$\Pi = U + W = U + W_1 + W_2 + W_3. \quad (7)$$

Where W_1 is the work done by the concentrated force in the AC section; W_2 is the work done by the component of gravity at the parallel level, and W_3 is the work done by the component of gravity at the perpendicular level. Bringing in the work in the three directions and the elastic strain energy, the total potential energy can be obtained as:

$$\Pi = EI \frac{\pi^4 a^2}{l^3} + P_{rc} \frac{\pi^2 a^2}{4l} + P_x \frac{\pi^2 a^2}{8} - \frac{P_y l a}{2}. \quad (8)$$

Bringing the potential energy standing value condition into the total potential energy equation and solving for the shape function, it can be derived based on the strength theory that the coal plate unit body reaches the ultimate deflection y_{\max} when $x = l/2$:

$$y_{\max} = \frac{4Pyl^4}{8\pi^4 EI + 2\pi^2 P_{rc} l^2 + \pi^2 P_x l^3}. \quad (9)$$

That is, the maximum value of the bending moment, M_{\max} , and the maximum value of the tensile stress, σ_{\max} , are obtained at the point of maximum deflection:

$$M_{\max} = y_{\max} P_{rc} + \int_0^{l/2} P_x (y_{\max} - y) dx + \int_0^{l/2} P_y \left(\frac{l}{2} - x \right) dx = y_{\max} P_{rc} + y_{\max} P_x \frac{l}{4} + P_y \frac{l^2}{8} \quad (10)$$

$$\sigma_{\max} = M_{\max} \frac{h}{2I} - \frac{P_{rc}}{A} - \frac{P_x}{A} = \frac{6M_{\max} - hP_{rc} - hP_x}{h^2} = f(l^*). \quad (11)$$

The research results illustrate that σ_{\max} is associated with the potential damage point l^* of the coal plate unit body, and when $\sigma_{\max} > \sigma_p$, the coal wall bending section undergoes tensile damage. Since coal wall rib spalling is an instantaneous process, the length of the coal wall bending section under its differential structural unit body cannot be accurately predicted, so the bending section l is assumed to be an unknown quantity, and the relevant physico-mechanical parameters (Table 1) are brought into the theoretical prediction model for verification.

The above parameters are substituted into Eqs. (10) and (11), and the results are calculated using mathematical software as shown in Fig. 5. With the continuous increase in tensile stress, the damage location point (l^*) of the coal wall increases approximately exponentially until it reaches the limit value corresponding to the tensile strength of the coal body, at which point damage initiates. The tensile strength range for field coal samples is situated between 0.7 ~ 1.1 MPa, with an average of 0.92 MPa, represented by point C in the figure. Prior to this calculation, the bottom of the band was initially stored at the bottom of the 1 m DB section. The tensile strength of the coal body reaches its critical point at C , where the maximum tensile stress causes damage at a distance of 3.5 m from the plate's bottom. After using the theoretical model established by the *Rayleigh-Ritz* method, the result is similar to the actual damage effect in the field, but there is still an error with some field phenomena. The reason for this may be that the brittle damage of the coal plate occurred before reaching the maximum tensile strength value, or the influence of other microstructural surfaces was neglected in the model, so further discussion is needed.

Analysis of numerical simulation results

Numerical simulation serves as a pivotal bridge between theoretical analysis and field observations, enabling the elucidation of the evolution mechanism of complex engineering problems in a shorter period. The use of simulation software to study the destruction process of the coal wall can better elucidate the rib spalling mechanism of the coal wall. Taking the 122,107 working face of the Caojiatan coal mine as the research background, numerical simulation was carried out to analyse the development process of the plastic zone of the coal wall, and the parameters of the model materials are shown in Table 2.

L/m	h/m	$\theta/^\circ$	$\gamma/(\text{kN}\cdot\text{m}^{-3})$	c/MPa	ϕ/MPa
6	1	85	24.5	0.042	25.35

Table 1. Mechanical parameters of coal wall rib spalling.

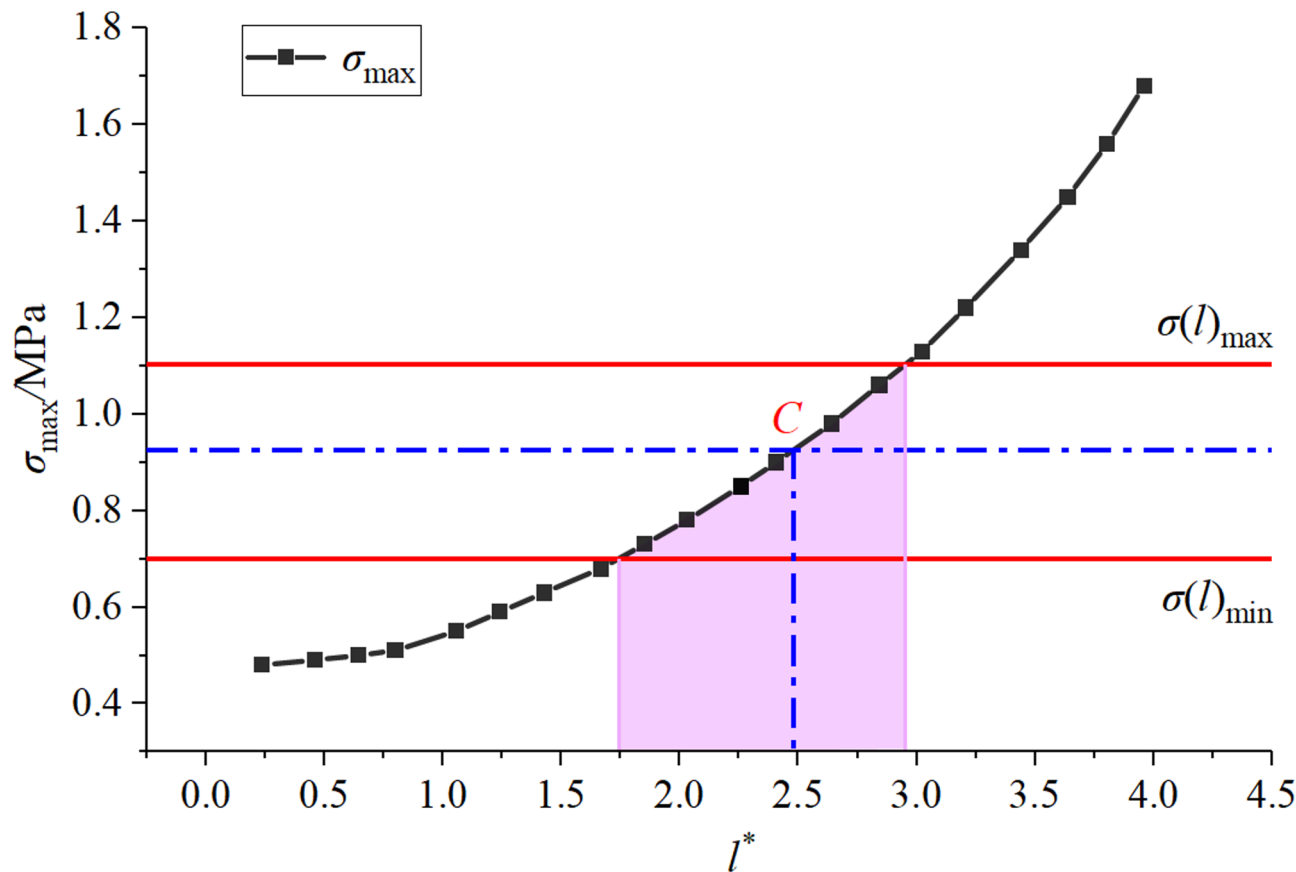


Fig. 5. Relationship between coal wall damage locations and maximum tensile stresses.

Rockiness	Density /(kg•m ⁻³)	Elastic modulus /GPa	Shear modulus /GPa	Cohesion /MPa	Tensile strength /MPa	internal friction angle /(°)
Sandstone	2400	4.1	3.7	8.4	2.5	39
Siltstone	2300	3.2	3.1	7.8	2.3	39
2-2 Coal	1250	1.2	0.9	4.5	1.5	38
Mudstone	2300	1.7	1.4	7.5	2.2	37
Siltstone	2350	2.8	2.6	8.4	2.5	39

Table 2. Model material parameters.

The numerical simulation model has dimensions of 200 m × 300 m × 80 m (width × length × height). The Mohr-Coulomb constitutive model was employed to describe the material behavior within the model. Boundary conditions were set as follows: fixed boundaries along the x-axis and y-axis, with the lower boundary of the z-axis also fixed. A vertical load of 7.51 MPa was applied to the top boundary of the z-axis, while a uniform horizontal pressure of 6.25 MPa was applied across the entire model. For the critical research area, specifically the No. 2-2 coal seam, a refined mesh was utilized to enhance the accuracy of the simulation results. Figures 6 and 7 illustrate the cross-sectional views of the model and the effects over time steps, respectively.

The time-step effect is a fundamental concept in numerical simulation, referring to the discretization of the simulated system over time. In the context of coal wall mining, the simulation's time step is progressively divided as the process evolves, allowing for convergence towards the true evolutionary behavior of the system. Within this model, the computational steps are set and dynamically adjusted to ensure that the simulation accurately reflects the spalling development process at various intervals, with the evolution trend of its plastic zone illustrated in Fig. 7 (b).

When calculating Fig. 7 (a), the simulation results can be seen that the working face 0.5~1 m from the roof plate firstly appears the plastic zone penetration. Analysing the reason, the soft structural surface in the coal body has low shear strength, and a shear plastic zone appears after reaching its limit value, with the increase of calculation steps, the area of the plastic zone gradually develops (Fig. 7b); after that, the area of plastic zone extends downward, and it reaches the maximum in the middle of the working face (Fig. 7c); the development of the plastic zone on the left and right side of the working face has a spatial penetration (Fig. 7d); with the

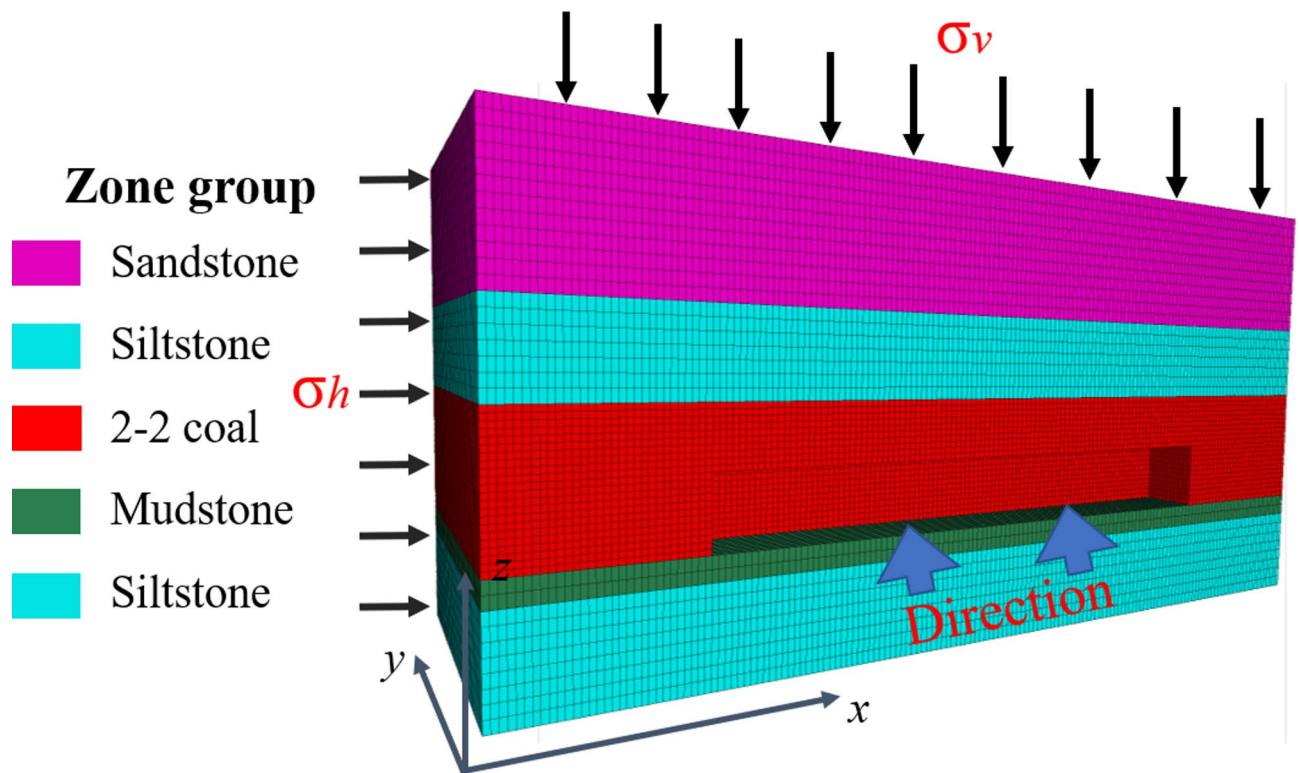


Fig. 6. Mesh Model Advancement Profile.

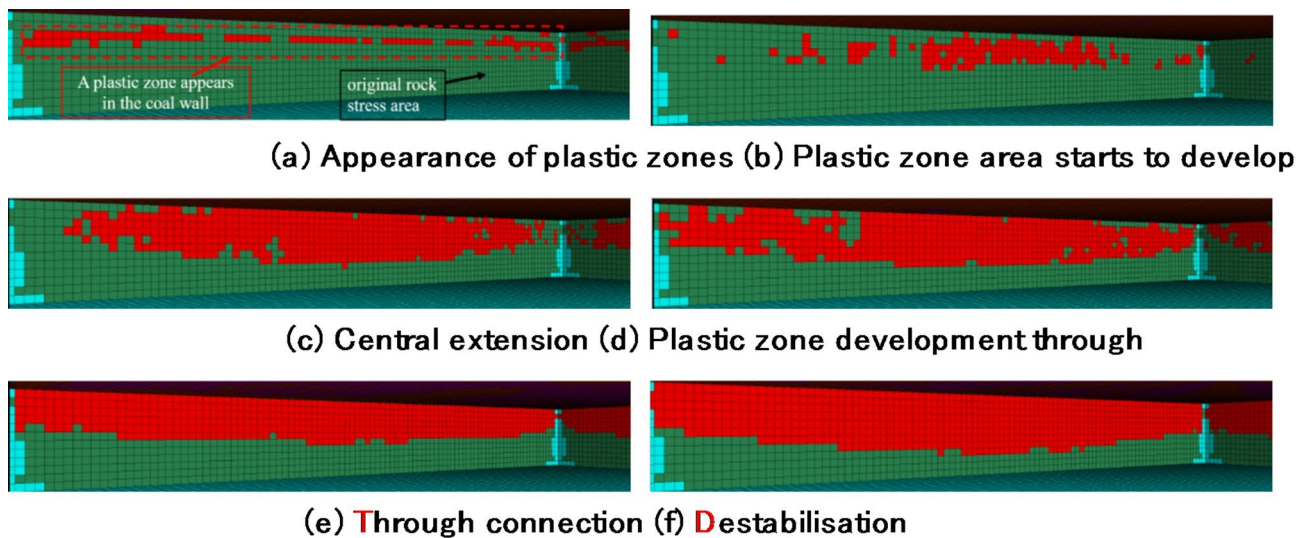


Fig. 7. Spatial development of plastic zone of coal wall.

continual extension of the plastic zone to the lower part, the unit slips along the smooth layer structural surface. Bending deformation occurs in the middle position, and the plastic zone is connected through (Fig. 7e); with the increase of bending deformation, the tensile plastic zone on the surface of the coal wall expands sufficiently and connects with the shear plastic zone, and finally the coal wall is unstable, and tensile cracking damages occur.

The numerical simulation results indicate that the plastic zone within the coal face initially develops in the upper-middle region before spreading toward the top and central sections, eventually impacting approximately two-thirds of the coal face's surface area. The spatial distribution of the plastic zone shows a distinctive pattern characterized by a broader central area that tapers off towards the ends, consistent with the spalling characteristics observed during field inspections. Moreover, theoretical analysis confirms that peak tensile stress-induced damage typically occurs around 2.5 m beneath the roof strata. This evidence supports the hypothesis that

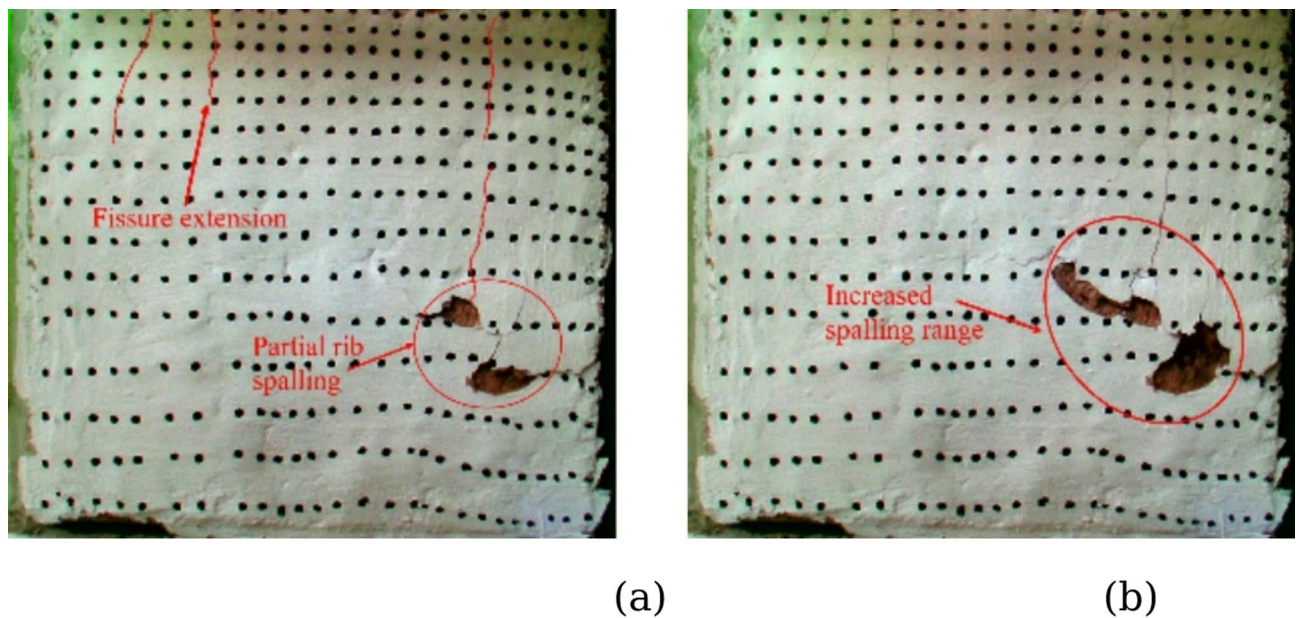


Fig. 8. Simulated test charts for similar materials.

deterioration of the coal face begins in the middle region and advances upward. The observed behavior aligns with the common tensile fracture mechanism associated with thick, hard coal seam spalling.

Similar simulation of coal wall spalling in large mining height working face

At present, domestic and international research into coal wall rib spalling primarily emphasizes theoretical analysis and numerical simulation, along with a limited number of two-dimensional planar physical models. However, there have been few three-dimensional experimental studies focusing on rib spalling in extra-thick hard coal seams. In light of this situation, three-dimensional similar material simulation experiments were conducted.

Tests were carried out using the three-dimensional similarity simulation test platform at the mine pressure similarity simulation laboratory³⁸. The test platform is an approximately long box type, the front section is equipped with an instrument placing platform, the total external dimensions of the platform box is 1.5 m×0.8 m×1.3 m, and the internal material filling box size is 0.8 m×0.8 m×0.6 m. Similar materials were prepared by mixing river sand, gypsum, and lime in a ratio of 50:5:5 by weight. Water was added to the mixture at 7% of the total weight, resulting in a solidified composite material with sufficient strength. The mechanical parameters of the coal body from the Caojiatan 1,222,107 working face served as the basis for the design of the experimental model. A geometric similarity ratio of 1:10 and a dynamic similarity ratio of 1:1.6 were adopted to ensure accurate representation of the in situ conditions.

The lateral deformation of the coal wall is crucial for assessing the extent of coal wall damage. In this experiment, a CCD industrial camera was utilized to monitor the surface displacement of the coal wall, with subsequent data export of surface point movement accomplished via numerical scattering software. The experimental loading system employs an equivalent fixed load method, incrementally increasing the load blocks to simulate actual mine pressure levels.

The development and damage law of coal wall fissures under equivalent concentrated force is shown in Fig. 8. At the initial stage of loading, fissures were generated at the junction of coal wall and roof; as the pressure of roof increases, the fissures on the surface of coal wall expand and penetrate, and the coal wall bulges outward obviously under the action of roof plate pressure, and the skin peels off in the middle, producing local rib spalling phenomenon (Fig. 8a, b); after that, the coal wall fissures and local rib spalling expand under the action of mine pressure, and spread from the middle of the model to the upper part, and the strength of the model was damaged and enhanced (Fig. 8c); with the expansion and penetration of the model fissures, a large area of rib spalling occurred in the right part of the model, the fissures began to spread to the left part, and the fissures expansion phenomenon appeared in the upper left coal wall (Fig. 8d); the whole coal wall after rib spalling is shown in Fig. 8(d).

Under loading, the initial manifestation was localized rib spalling in the coal wall's midsection. As the fissures expanded and penetrated, deformation and structural instability ensued within the coal wall. Upon reaching the limit value for structural instability, rapid accumulation of smaller vertical and horizontal deformations led to overall rib spalling along the working face coal wall under loading. This motion sequence aligns with the theoretical slabbing-bending derivation previously discussed.

During testing, strain gauges were embedded within the coal body and connected to the DH3816 static strain test system for data to the transmission to a computer. Through software analysis, the strain value were recorded

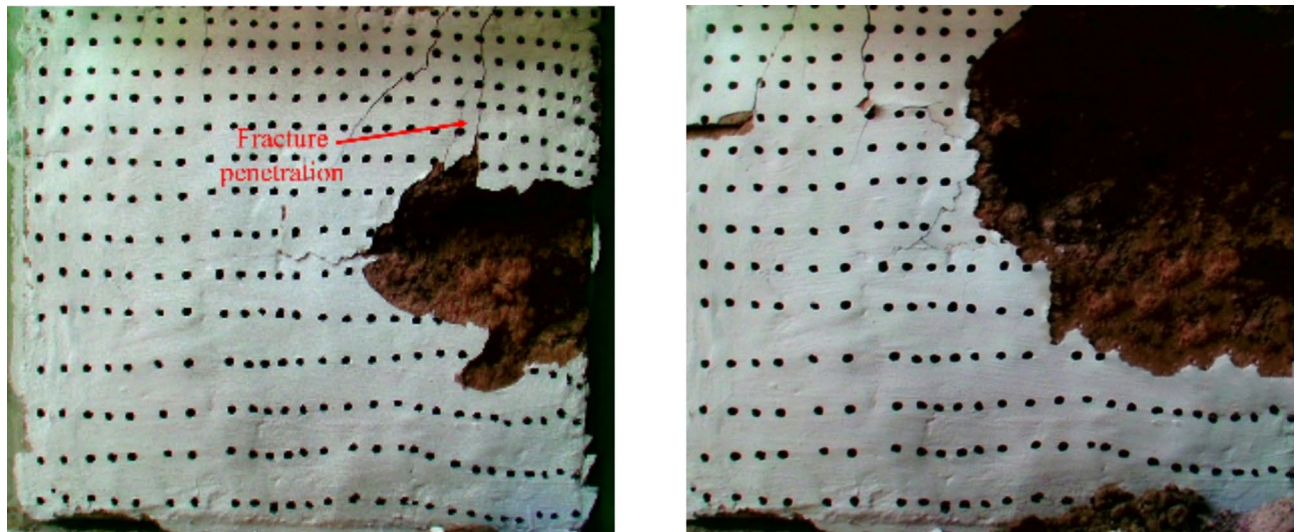


Fig. 8. (continued)

and subsequently converted into stress data during post-processing. Studying stress changes facilitates a deeper understanding of the coal body behavior. The layout of the strain gauge measurement points is shown in Fig. 9.

The stress measurement point data were extracted, and the stress change graph of the measurement point under different coal wall pressures was obtained after collation and calculation, as shown in Fig. 10. The graph curve shows an overall upward trend with the increase of coal wall roof pressure, the front part of the curve grows linearly, and the back end tends to flatten, the coal wall is destroyed after reaching the limit pressure it can withstand, and the curve undergoes a rapid decline, but the residual coal body has part of the strength, and the internal strain points of the coal body still retain their values.

When the working face is loaded with pressure, the change of its measuring point is shown in Fig. 10. The maximum point of stress change in the upper part is A5, with the maximum value of 5.59 MPa; the maximum point of stress change in the middle measuring point is B4, with the maximum value of 5.58 MPa; the maximum value of change in the lower part is C2, with the maximum value of 5.61 MPa. Comparison of the stress change reveals that the stress change in the upper part of the measuring point is generally higher than that in the middle and in the lower part of the model, and the change in the middle part of the model is generally higher than that in the two ends. The stress change in the middle of the model is generally larger than that in the two ends. The maximum stress change of the whole model is A2. Combined with the analysis of the coal wall rib spalling pattern in Fig. 8, it can be seen that the working face was cracked in the middle and then the cracks in the body quickly penetrated to the upper part, and then destabilization occurred.

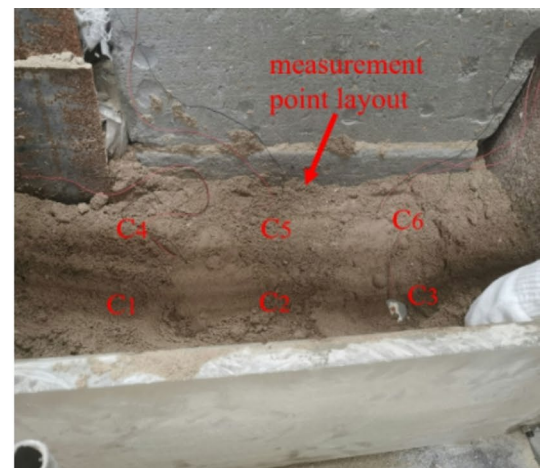
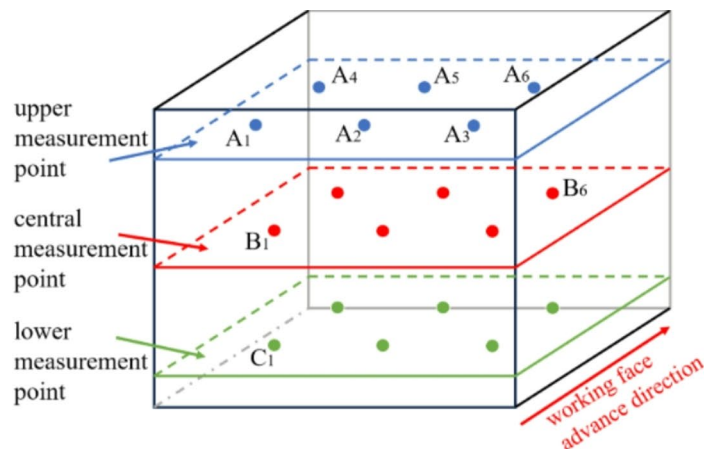


Fig. 9. Test Strain Gauge Point Arrangement.

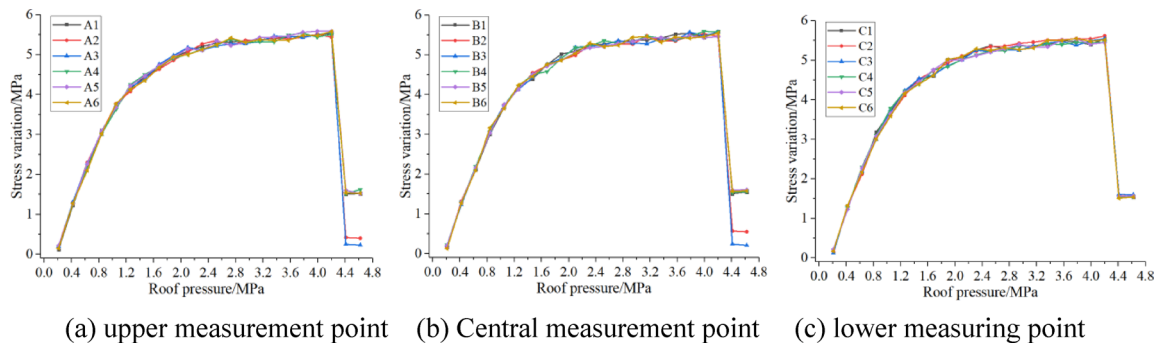


Fig. 10. Plot of stress changes at coal wall measurement points.

Conclusion

- (1) Based on the characteristics of hard coal rib spalling observed in the field, the movement process of rib spalling has been subdivided into three phases: dynamic loading influence, crack propagation, and flexural instability. A comprehensive mechanical model for the entire structure and a specific model for the bending section were established according to the deformation evolution mechanism of stratified tensile cracking in the coal rib. The displacement formula for coal rib spalling was derived using the Rayleigh-Ritz method, the principle of stationary potential energy, combined with beam plate strength theory and maximum tensile stress strength theory.
- (2) Mathematical analysis software was employed to calculate the relationship between the location of coal rib damage and the maximum tensile stress. Incorporating the specific parameters of the mine, it was deduced that the maximum tensile stress damage in the coal rib of the 122,107 face occurs approximately 2.5 m below the roof. Considering the time step effect, numerical simulations were used to analyze the full development process of the plastic zone in the coal rib. The results indicate that substantial tensile cracking failure is predominant in thick hard coal rib spalling.
- (3) Similarity simulation experiments revealed that cracks initiate from the middle-upper part of the coal rib and propagate upwards, leading to rib spalling. The trajectory of rib spalling can be described as originating from mid-rib cracks that trigger localized spalling which rapidly evolves into overall spalling. Strain measurement analyses demonstrated that after experiencing strength instability, the coal rib undergoes structural instability. The overall research findings provide technical references for prevention and control of similar mine rib spalling and offer theoretical foundations for calculating the breakage location of coal ribs in analogous working faces.

Recommendations

The findings obtained in this study, including the detailed subdivision of the coal rib spalling movement process and the derivation of the coal rib spalling displacement using theories such as the Rayleigh-Ritz method and the principle of stationary potential energy, lay a foundation for future research. It is hoped that more scholars will investigate thick hard coal rib spalling from diverse perspectives to achieve a more precise determination of the coal rib breakage location and a more accurate description of the spalling characteristics. Moreover, while the three-dimensional similarity simulation experiments in this study simplified the immediate roof as a rigid structure subjected to continuous loading, it should be noted that the impact of dynamic loading due to face advance is also a critical factor in the field. Future studies should aim to refine the modeling of the roof structure in 3D similarity simulations to better replicate actual site conditions, thereby obtaining simulation results that more closely mimic real-world scenarios.

Data availability

The datasets used and/or analysed during the current study available from the corresponding author on reasonable request.

Received: 9 October 2024; Accepted: 25 June 2025

Published online: 23 July 2025

References

1. Yang, T., Xia, H., Meng, X. & Kuang, T. Failure mechanism of the large-section roadway under mined zones in the ultra-thick coal seam and its control technology. *Energy Sci. Eng.* <https://doi.org/10.1002/ese3.564> (2019).
2. Bai, Q., Wang, T. & Zhang, F. Field and numerical investigations of gateroad system failure induced by hard roofs in a Longwall top coal caving face. *Int. J. Coal Geol.* **173**, 176–199 (2017).
3. Zhu, D. F. et al. Numerical investigation of particles flow pattern and pressure distribution of coal bunker. *J. Geophys. Eng.* **20** (4), 841–853. <https://doi.org/10.1093/jge/gxad052> (2023).
4. Xiong, Y., Kong, D. Z. & Song, G. Research hotspots and development trends of green coal mining: exploring the path to sustainable development of coal mines. *Resour. Policy*. **92**. <https://doi.org/10.1016/j.resourpol.2024.105039> (2024).

5. Cheng, Z. B., Yang, S. L., Li, L. H. & Zhang, L. F. Support working resistance determined on top-coal caving face based on coal-rock combined body. *Geomech. Eng.* **19** (3), 255–268. <https://doi.org/10.12989/gae.2019.19.3.255> (2019).
6. Takaishvili, L. & Sokolov, A. Coal industry of East Siberia-prospects for development, *International conference regional energy policy of Asian RUSSIA*, Irkutsk, RUSSIA, April. (2019). <https://doi.org/10.1051/e3sconf/20197703001>
7. Xue, B., Wang, C., Wang, Y., Zhang, W. & Yang, S. An investigation of the coal wall zoning failure patterns resulting from the changes in support parameters of large mining height. *Mech. Time-Dependent Mater.* 1–20. <https://doi.org/10.1007/s11043-023-09660-6> (2023).
8. He, F. L., Gao, S., Zhang, G. C. & Jiang, B. Y. Ground response of a gob-side gateroad suffering mining-induced stress in an extra Thick coal seam. *Geomech. Eng.* **22** (1), 1–9. <https://doi.org/10.12989/gae.2020.22.1.001> (2020).
9. Modi, P., Jamal, A. & Singh, N. Coal characterization and occurrence of rare Earth elements in coal and coal-ash of Sohagpur coalfield, Madhya Pradesh, India. *Int. J. Coal Preparation Utilization.* **42** (10), 2976–2989. <https://doi.org/10.1080/19392699.2021.1923489> (2021).
10. Bae, J. S. et al. Improvement in coal content of coal-water slurry using hybrid coal impregnated with molasses. *Powder Technol.* **254**, 72–77. <https://doi.org/10.1016/j.powtec.2013.12.032> (2014).
11. Yang, H. Y. et al. A caving self stabilization bearing structure of advancing cutting roof for gob-side entry retaining with hard roof stratum. *Geomech. Eng.* **21** (1), 23–33. <https://doi.org/10.12989/gae.2020.21.1.023> (2020).
12. Wei, W. J., Yang, S. L., Li, M., Zhang, J. W. & Wei, C. B. Motion mechanisms for top coal and gangue blocks in Longwall top coal caving with an extra Thick seam. *Rock Mech. Rock Eng.* **55** (8), 5107–5121. <https://doi.org/10.1007/s00603-022-02928-2> (2022).
13. Gao, R., Kuang, T. J. & Lan, Y. W. The mechanism and control technology of strong strata behavior in extra Thick coal seam mining influenced by overlying coal pillar. *Open. Geosci.* **11** (1), 452–461. <https://doi.org/10.1515/geo-2019-0036> (2019).
14. Kumar, A., Kumar, D., Singh, A. K., Ram, S. & Kumar, R. Development of empirical model for strength Estimation of irregular-shaped-heightened-rib/snook for mechanised depillaring. *Int. J. Rock Mech. Min. Sci.* **148**, 104969. <https://doi.org/10.1016/j.jrmms.2021.104969> (2021).
15. Sinha, S. & Walton, G. Modeling behaviors of a coal pillar rib using the progressive S-shaped yield criterion. *J. Rock Mech. Geotech. Eng.* **12** (3), 484–492. <https://doi.org/10.1016/j.jrmge.2019.12.002> (2020).
16. Yetkin, M. E. & Simsir, F. Determination of most suitable working height of powered roof support considering roof stresses. *J. Min. Sci.* **55** (1), 23–30. <https://doi.org/10.1134/S1062739119015251> (2019).
17. Jirankova, E. & Lazecsky, M. Ground surface uplift during subsidence trough formation due to Longwall mining in the shaft protection pillar of the CSM mine. *Bull. Sci. Geol. Environ.* **81** (9), 389. <https://doi.org/10.1007/s10064-022-02896-5> (2022).
18. Mondal, D., Roy, P. N. S. & Kumar, M. Monitoring the strata behavior in the distressed zone of a shallow Indian Longwall panel with hard sandstone cover using Mine-Microseismicity and borehole televiewer data. *Eng. Geol.* **271**, 105593. <https://doi.org/10.1016/j.enggeo.2020.105593> (2020).
19. Yuan, Y., Tu, S. H., Wang, F. T., Zhang, X. G. & Li, B. Hydraulic support instability mechanism and its control in a fully-mechanized steep coal seam working face with large mining height. *J. South Afr. Inst. Min. Metall.* **115** (5), 441–447 (2015).
20. Yuan, Y., Tu, S. H., Ma, X. T., Sun, L. L. & Bai, Q. S. Coal wall stability of fully mechanized working face with great mining height in ‘three soft’ coal seam and its control technology. *J. Min. Saf. Eng.* **29** (1), 21–25 (2012).
21. Yin, X. W., Yan, S. H. & An, Y. Characters of the rib spalling in fully mechanized caving face with great mining height. *J. Min. Saf. Eng.* **25** (2), 222–225 (2008).
22. Li, X. P., Kang, T. H. & Yang, Y. K. Analysis of coal wall slip risk and caving depth based on bishop method. *J. China Coal Soc.* **25** (2), 222–225. <https://doi.org/10.13225/j.cnki.jccs.2014.0912> (2015).
23. Pang, Y. H., Wang, H. B., Zhao, J. J. & Shang, D. Y. Analysis and Prediction of Hydraulic Support Load Based on Time Series Data Modeling. *Geofluids*, 2020:8851475. (2020). <https://doi.org/10.1155/2020/8851475>
24. Wang, G. F., Pang, Y. H., Li, M. Z., Ma, Y. & Liu, X. H. Hydraulic support and coal wall coupling relationship in ultra large height mining face. *J. China Coal Soc.* **42** (2), 518–526. <https://doi.org/10.13225/j.cnki.jccs.2016.0699> (2017).
25. Xu, X., Kong, D. Z., Xiong, Y. & Chen, F. Evolution regularity and control technology of coal face rupture induced by the movement of overlying strata under the influence of mining. *Min. Metall. Explor.* **40** (1), 435–452. <https://doi.org/10.1007/s42461-022-00716-8> (2022).
26. Kong, D. Z. et al. Stability analysis of coal face based on coal face-support-roof system in steeply inclined coal seam. *Geomech. Eng.* **25** (3), 233–243. <https://doi.org/10.12989/gae.2021.25.3.233> (2021).
27. Wang, J. C. et al. A new method for improving coal wall stability in Longwall mining by considering support stiffness. *Bull. Eng. Geol. Environ.* **85** (5), 163. <https://doi.org/10.1007/s10064-023-03179-3> (2023).
28. Shen, B. T. & Barton, T. Rock fracturing mechanisms around underground openings. *Geomech. Eng.* **16** (1), 35–47. <https://doi.org/10.12989/gae.2018.16.1.035> (2018).
29. Liu, H. T. et al. Coal wall spalling mechanism and grouting reinforcement technology of large mining height working face. *Sensors* **22** (22), 8675. <https://doi.org/10.3390/s22228675> (2022).
30. Zeng, Q., Ma, X., Wan, L., Zhu, Y. & Yue, Y. Research on the hydraulic support face guard mechanism and coupling characteristic of rib spalling in large mining heights. *Sci. Rep.* **14** (1), 8110. <https://doi.org/10.1038/s41598-024-58542-5> (2024).
31. Si, L., Wang, Z. B., Liu, X. H., Tan, C. & Xu, R. X. Assessment of rib spalling hazard degree in mining face based on background Subtraction algorithm and support vector machine. *Curr. Sci.* **116** (12), 2001–2012. <https://doi.org/10.18520/cs/v116/i12/2000-2012> (2019).
32. Li, W., Ye, Y. H., Wang, Q. H., Wang, X. H. & He, N. Y. Fuzzy risk prediction of roof fall and rib spalling: Based on FFTA-DFCE and risk matrix methods. *Environmental Sci. Pollution Res.* **27** (8), 8535–8547. <https://doi.org/10.1007/s11356-019-06972-4> (2020).
33. Sun, J., Li, B., Zhang, R. F. & Huang, Z. Feasibility of Water Injection on the Coal Wall of Loose Thick Coal Seam to Prevent Rib Spalling and Its Optimal Moisture Content. *Geofluids*, 2022:5733695. (2022). <https://doi.org/10.1155/2022/5733695>
34. Xiang, Y., Wei, W. J., Zhang, L., Li, M. Z. & Wu, S. X. Stability analysis and failure control of a Longwall panel with a large mining height considering fracture distribution. *Bull. Eng. Geol. Environ.* **82** (2), 54. <https://doi.org/10.1007/s10064-022-03052-9> (2023).
35. Zhang, G. C., He, F. L., Jiang, H. G. & Lai, Y. H. Analysis of gateroad stability in relation to yield pillar size: A case study. *Rock Mech. Rock Eng.* **50** (5), 1263–1278. <https://doi.org/10.1007/s00603-016-1155-1> (2017).
36. Fan, J. Y. et al. A stress model reflecting the effect of the friction angle on rockbursts in coal mines. *Geomech. Eng.* **18** (1), 21–27. <https://doi.org/10.12989/gae.2019.18.1.021> (2019).
37. Xu, Y. X., Wang, G. F., Li, M. Z., Zhang, J. H. & Han, H. J. Structure coupling between hydraulic roof support and surrounding rock in extra-thick and hard coal seam with super large cutting height and Longwall top coal caving operation. *J. China Coal Soc.* **44** (6), 1666–1678. <https://doi.org/10.13225/j.cnki.jccs.2019.0073> (2019).
38. Xue, B., Zhang, W. & Wang, C. Determination of working resistance of support parameter variation of large mining height support: the case of Caojiatan coal mine, *Geomechanics and Geophysics for Geo-energy and Geo-resources* 10(1), 297–315. (2024). <https://doi.org/10.1007/s40948-023-00730-0>

Acknowledgements

Financial support for this work was provided by the Erdos Mining Area Geohazard Prevention and Geoenvironmental Protection Engineering Research Center (No. RZ2300001544), the National Natural Science Foundation

of China (No.52174072), the National Natural Science Foundation of China (No.52364010), Inner Mongolia Natural Science Foundation (No.2025QN5109), Youth Talent Support Program under the Ordos Science and Technology Plan (No.RC20250115). The authors gratefully acknowledge the financial support from the organizations mentioned above.

Author contributions

Data analysis and collection, B. Xue, and Yunfei Liu; methodology, B. Xue; writing-original draft preparation, B. Xue; writing-review and editing, B. Xue; supervision, C. Wang, and F.T. Zhang; project administration, Y. Shang, and C. Wang; funding acquisition, Y. Shang, and C. Wang.

Declarations

Ethics approval and consent to participate

No approval of research ethics committees was required to accomplish the goals of this study because experimental work was conducted with an unregulated species.

Consent for publication

Not applicable for this section.

Competing interests

The authors declare no competing interests.

Conflict of interest

The authors declare that they have no known competing financial interests or personal relationships that could have appeared to influence the work reported in this paper.

Additional information

Correspondence and requests for materials should be addressed to B.X.

Reprints and permissions information is available at www.nature.com/reprints.

Publisher's note Springer Nature remains neutral with regard to jurisdictional claims in published maps and institutional affiliations.

Open Access This article is licensed under a Creative Commons Attribution-NonCommercial-NoDerivatives 4.0 International License, which permits any non-commercial use, sharing, distribution and reproduction in any medium or format, as long as you give appropriate credit to the original author(s) and the source, provide a link to the Creative Commons licence, and indicate if you modified the licensed material. You do not have permission under this licence to share adapted material derived from this article or parts of it. The images or other third party material in this article are included in the article's Creative Commons licence, unless indicated otherwise in a credit line to the material. If material is not included in the article's Creative Commons licence and your intended use is not permitted by statutory regulation or exceeds the permitted use, you will need to obtain permission directly from the copyright holder. To view a copy of this licence, visit <http://creativecommons.org/licenses/by-nc-nd/4.0/>.

© The Author(s) 2025